Mathematical Model and Parameter Estimation for Gas-Phase Ethylene Homopolymerization With Supported Metallocene Catalyst

ARTICLE *in* INDUSTRIAL & ENGINEERING CHEMISTRY RESEARCH · FEBRUARY 2005

Impact Factor: 2.59 · DOI: 10.1021/ie048957o

5 AUTHORS, INCLUDING:

Kimberley McAuley
Queen's University
146 PUBLICATIONS **3,201** CITATIONS
SEE PROFILE

David W. Bacon
Queen's University
65 PUBLICATIONS **1,251** CITATIONS
SEE PROFILE

Mathematical Model and Parameter Estimation for Gas-Phase Ethylene Homopolymerization with Supported Metallocene Catalyst

Bo Kou,† Kim B. McAuley,* C. C. Hsu, David W. Bacon, and K. Zhen Yao‡

Department of Chemical Engineering, Queen's University, Kingston, Ontario, Canada K7L 3N6

A dynamic model for gas-phase ethylene homopolymerization using a supported metallocene catalyst is developed in this work. A single-site model was first developed, with model parameters estimated from measurements from 11 experimental runs in a semibatch laboratory-scale reactor. Estimability analysis techniques were applied to aid in the parameter estimation. Although the single-site model provided good fits for both the polymerization rate and hydrogen concentration, it failed to accurately predict the molecular weight data and its distribution. Sequentially, a simplified two-site model was built to improve model predictions. The two-site model, which used three additional parameters, showed significant improvements over the single-site model. The two-site model was validated using the data from two extra experimental runs, which were not employed in the parameter estimation process. Most of the model predictions fall within the 95% confidence intervals of the experimental data.

Introduction

Gas-phase ethylene polymerization with supported metallocene catalysts is a very complex process and involves a great number of chemical reactions and physical phenomena. To fundamentally describe and simulate this process, complicated mechanistic models are usually required, which may result in highly stiff, coupled differential equations and many unknown parameters. Although many mechanistic models have been developed to describe low-pressure ethylene polymerization, parameter estimation is such a difficult problem that it is uncommon to find models with parameters that have been estimated using experimental data. Most modelers obtain approximate values of model parameters from the literature or assume them arbitrarily.[1−7] Although these models can give qualitative explanations of important phenomena during ethylene polymerization and qualitative predictions of the relationships between operating conditions and polymer properties, no experiments have been used to verify these explanations and predictions.

Recently, new techniques have been developed to aid parameter estimation in mathematical models for metallocene and Ziegler−Natta catalyzed olefin polymerization models[8−13] so that reasonable parameter values can be used in reactor simulators. Khare et al.[8,9] developed a manually implemented iterative parameter-estimation methodology and applied it to isothermal models of high-density polyethylene[8] and polypropylene[9] production. They began by adjusting a small number of parameters in a single-site model to match steady-state polymerization rate, comonomer incorporation, and number-average molecular weight data. In subsequent steps, they deconvoluted experimental steady-state molecular weight distributions to determine the number of active sites required in their model. They manually adjusted a small number of chain-transfer rate constants at individual active sites to match the corresponding number-average molecular weights corresponding to each type of active site. Their technique required that they consider each grade one at a time, adjusting parameters manually to ensure that they could match the production rate, number-average molecular weight, and polydispersity data for each new grade in their data set. Matos et al.[10,11] developed a different technique for determining parameters in fundamental low-pressure polyolefin reactor models. They used gel permeation chromatography (GPC) deconvolution of steady-state data to determine the number of active sites required in their nonisothermal models for bulk propylene polymerization and fitted simplified kinetic expressions for each site type, making every effort to keep the number of model parameters to a minimum, while ensuring that their model parameters were consistent with GPC data and NMR sequence data. After fitting the parameters that influenced steady-state product properties, Matos et al. were able to fit a limited number of catalyst activation and deactivation parameters using dynamic rate profiles. Instead of adjusting their parameters manually, Matos et al. were able to sufficiently simplify their model equations so that nonlinear least-squares estimation could be used for parameter estimation in their various submodels. A major focus of their work is good experimental design to ensure that all of the parameters in their simplified models can be determined from the experimental data.

More recently, Yao et al.[12] and Li et al.[13] have developed estimability analysis techniques that enable automated estimation of parameters in complex olefin polymerization models, using limited experimental data. The idea is to determine subsets of the model parameters that can be estimated using the available data and to estimate only these parameters. In these estimability analysis techniques,[12,13] a parametric sensitivity matrix

* To whom correspondence should be addressed.

† Current address: DuPont Canada Inc., Research and Business Development Center, Kingston, Ontario, Canada K7L 5A5.

‡ Current address: Institute of Polymerization Reaction Engineering, Zhejiang University, Hangzhou, China 310027.

10.1021/ie048957o CCC: $30.25
Published on Web 02/24/2005

Table 1. Operating Conditions of Homopolymerization Used for Parameter Estimation

run	run time min	temperature °C	pressure psi	$[H_2]$ mol %	catalyst g	MAO mol/mol	scavenger g	run no.[a]
1	210	60	160	0.4	0.2	400	0.3	2
2	***30***	***60***	***100***	***0.8***	***0.4***	***1200***	***0.9***	7
3	30	60	100	0.8	1	1200	0.9	7a
4	50	85	160	0.8	0.4	400	0.3	6
5	30	85	100	0.5	0.2	1200	0.9	3
6	***30***	***85***	***100***	***0.4***	***0.4***	***400***	***0.3***	12
7	210	85	160	0.8	0.2	400	0.3	6a
8	480	85	100	0.88	0.3	1200	0.3	8hr
9	120	85	100	0.2	0.1	1200	0.0	S13
10	30	60	160	0.2	0.04	1200	0.0	S10
11	30	60	160	0.2	0.04	2245	0.0	S12
12	30	72.5	130	0	0.30	800	0.0	S2
13	90	72.5	130	0	0.15	800	0.0	S3

[a] References 14 and 15.

is used to provide information about the influence of each model parameter on the various model predictions and about correlation between the effects of different parameters. The parameters that are selected for estimation are updated from their initial values using nonlinear least-squares, and the remaining parameters are left at their initial values or, if desired, can be removed from the model via subsequent model simplification. Estimability analysis can also be used as an aid for designing additional experiments aimed at getting improved estimates of key parameters that are not estimable from an initial data set. Yao et al.'s estimability analysis method readily accommodates dynamic models and dynamic data, as well as response variables that are available at different sampling rates throughout each experimental run, whereas the method of Li et al.[13] does not. The main benefits of the estimability methods,[12,13] compared with the approaches of Khare et al.[8,9] and Matos et al.,[10,11] are that no manual adjustment of parameters and no a priori simplification of the model equations are required, and less insight into which mechanisms are important and which can be neglected is needed, before parameters can be estimated. Also, careful experimental design is not such an important issue. If the initial data have little information about some parameters, these parameters are automatically excluded from the parameter estimation, so that problems related to ill-conditioning problems do not arise. Subsequent experiments can be designed to get estimates of parameters that were not initially estimable.[12] One of the disadvantages that may arise when using the all-at-once estimability analysis approach to parameter estimation rather than the methods of Khare et al.[8,9] and Matos et al.[10,11] is that identification of sources of lack-of-fit may become more difficult when there are deficiencies in the model structure.

In the current article, we use the estimability analysis techniques of Yao et al.[12] to aid in parameter estimation. Mathematical models are developed to simulate gas-phase ethylene homopolymerization using a supported metallocene catalyst in a semibatch laboratory-scale reactor. The reactor system used to conduct the experiments is described, followed by the development of a single-site model. Subsequently a two-site model is developed because the single-site model is not able to predict the experimentally observed polydispersities. Finally experimental data that were not used for parameter estimation are used to test the validity of the model predictions.

Experimental System and Data

A series of semibatch ethylene homopolymerization runs (in Table 1) and copolymerization runs was conducted for parameter estimation and model validation using a 2L gas-phase reactor.[14,15] Before each experiment, salt bed, scavenger, cocatalyst, hydrogen, and ethylene were added into the reactor. Then, catalyst was blown into the reactor by ethylene to start polymerization. The reactor is operated isothermally by controlling the flow of cooling water and steam to the reactor jacket. The total pressure within the reactor was maintained by feeding ethylene to the reactor. Hydrogen was also fed to the reactor in a fixed ratio to the ethylene feed rate during each run. Up to 15 gas samples were collected during each run and were analyzed for hydrogen fraction by gas chromatography. At the end of each run, the polymer was removed from the reactor and analyzed for number- and weight-average molecular weight using high-temperature GPC.

The catalyst employed in this work was $(n\text{-BuCp})_2ZrCl_2$ (from Aldrich) supported on silica (0.0000192 molZr/gCat). The cocatalyst is MAO (10 wt % in toluene from Aldrich). Triisobutyl aluminum (25 wt % in toluene from Aldrich) was used as a scavenger and added to the reactor before polymerization to remove impurities. Ethylene (Polymer Grade) and hydrogen (Untra High Purity) were purchased from Praxair. In each run, 140 g of sodium chloride (≥99% from Sigma) was used as a salt bed to help catalyst dispersion.

Many of the experiments[14,15] shown in Table 1 are homopolymerization runs from a 12-run Plackett–Burman screening design that was used to identify the relative importance of reactor operating conditions on product properties and catalyst activities, arising from ethylene homopolymerization and ethylene/hexene copolymerization experiments. A set of sequential experiments that was conducted to study the effects of the scavenger on catalyst activity is also included. Within the homopolymerization runs, three types of rate profiles were observed as shown in Figure 1.

1. Experiments having relatively high activity and no rate increase at long reaction times. These experiments usually have relatively high catalyst activity (200−300 gPE/gCat·100psi·h) compared to the type 2 homopolymerization experiments (40−90 gPE/gCat·100psi·h), which also have no rate increase. These type 1 polymerization rate profiles increase directly to the peak rate during the first several minutes of reaction and then gradually decrease, due to deactivation of active sites. There is no induction period.

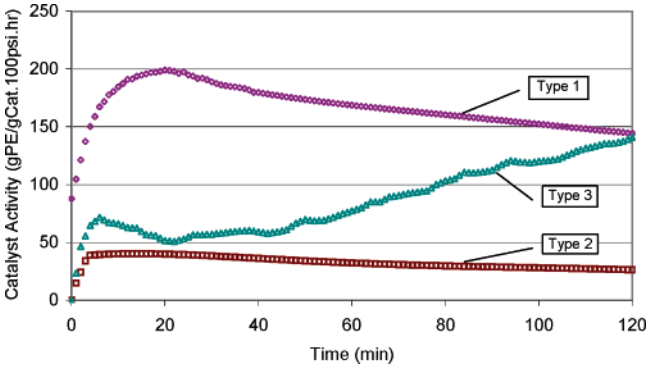

Figure 1. Types of polymerization rate profiles encountered in metallocene-catalyzed ethylene homopolymerization experiments.

2. Experiments having relatively low activity and no rate increase at long reaction times. The catalyst activity in these runs was usually below 100 gPE/gCat·100psi·h, and sometimes only very small catalyst deactivation was observed.

3. Experiments exhibiting a rate increase at long reaction times and not reaching the peak activity before the end of the experiment. In these experiments, the run time was not long enough for the process to reach the peak activity. The catalyst activity for these experimental runs varied from 50 to 300 gPE/gCat·100psi·h at the end of the experiment. A small peak also appears at the beginning of the polymerization for some of these runs.

Although the type 2 and type 3 profiles look different, they may be qualitatively the same, with the experiment ending at different stages of the rate profile, or they may be qualitatively different. The first type of rate profile, with high activity and no rate increase, is qualitatively distinct from the type 3 profile, because there is no induction period before reaching the maximum rate.

It has been shown that scavenger and temperature are the two most important factors that influence whether there is a low initial rate followed by a rate increase.[14] The models developed using the mechanism outlined herein are able to fit and predict rate curves of types 1 and 2 but not type 3, presumably because mechanisms that are important when both the scavenger level is very high and temperature is low are not included in the model. Experiments with high scavenger levels that exhibited rate increases (type 3 rate profiles)[14] were excluded from our modeling efforts because no plausible mechanism has been developed that can predict the type 3 profiles, as well as types 1 and 2. The high scavenger levels associated with the type 3 profiles were chosen to consume impurities that might be present in our laboratory-scale polymerization reactor. These high scavenger levels would not be encountered in industrial gas-phase polyethylene reactors.

The 13 homopolymerization runs[14] with rate profiles of types 1 and 2 (no delayed rate increase) were selected and used for modeling. Eleven runs were used for parameter estimation, and two runs (runs 2 and 6) were saved for model verification, so that the capability of the model to predict data that were not used for model fitting could be assessed. Runs 2 and 6 were selected because of their very different settings for important operating conditions (i.e., different temperatures, scavenger and cocatalyst levels, and hydrogen concentrations).

Single-Site Model

To develop the homopolymerization model, several basic assumptions were made, including the following:

i. Terminal model. The reactivity of the growing polymer chains depends only on the monomer bound in the chain next to the active site.

ii. Perfect agitation. This assumption allows us to develop a model with uniform temperature and reactant concentrations throughout the continuous gas phase in the reactor. Screening experiments using our semibatch laboratory reactor showed that the stirring speed had no significant effect on the polymerization rate or polymer properties.

iii. Instantaneous phase equilibrium and negligible heat and mass transfer resistances. This assumption allows us to treat all reaction rates as kinetically, rather than diffusionally, controlled and to assume uniform temperatures and reactant compositions throughout the polymer particles. Floyd et al.[16−20] used multigrain models to study the phase equilibrium of reactants between the gas phase and the amorphous polymer phase and the effects of mass- and heat-transfer resistances inside the polymer particles. Their research shows that the heat- and mass-transfer resistances both at the external film and inside particles can be considered negligible when the catalyst activity is below 4000 gPE/gCat·100psi·h. Since the activity of the metallocene catalyst was well below this value, it is reasonable to assume that transfer resistances are negligible, both inside the particles and between the gas phase and the amorphous polymer phase.

iv. Arrhenius behavior. The effects of temperature on all kinetic constants are assumed to follow Arrhenius behavior.

v. Henry's law. Polyethylene is a semicrystalline polymer containing amorphous and crystalline regions. The catalyst sites are surrounded by amorphous polymer, because the polymer must grow away from the catalyst surface before crystallizing. Concentrations of ethylene and hydrogen in the amorphous phase are proportional to their respective concentrations in the gas phase.[21,22]

vi. Gas inflow and outflow. It is assumed that as ethylene and hydrogen are consumed by reaction, a gas mixture with a specified hydrogen-to-ethylene ratio, r_{HM}, is fed to the reactor to ensure that the pressure remains constant. Since the quantities of ethylene and hydrogen gas removed from the reactor for GC analysis are very small (approximately 0.7% of the gas in the reactor is removed for each sample taken) compared to the quantities of makeup gas added during each run, the effect of sample removal on gas composition can be neglected.

vii. Negligible ethylene and hydrogen absorbed by the polymer. The amounts of ethylene and hydrogen dissolved in the amorphous polymer phase are small in comparison with the amount in the gas phase and can therefore be neglected in the material balance on ethylene and hydrogen.

viii. Neligible polymer volume. It is assumed that the polymer volume is negligible in comparison with total reactor volume. Therefore, the gas-phase volume is constant during reaction.

ix. Elementary reactions. All reactions are assumed to be elementary, indicating that the reaction order is the same as the number of participating molecules in

Table 2. Reaction Mechanisms of the Single-Site Homopolymerization Model

active site formation	$N^* + A \xrightarrow{k_{FDC}} N(0)$
active site initiation	$N(0) + M \xrightarrow{k_i} N_1(1)$
propagation	$N(r) + M \xrightarrow{k_{P1}} N(r+1)$
chain transfer	
transfer to cocatalyst	$N(r) + A \xrightarrow{k_{tA}} N_A(0) + Q(r)$
transfer to scavenger	$N(r) + S \xrightarrow{k_{tS}} N_S(0) + Q(r)$
transfer to hydrogen	$N(r) + H_2 \xrightarrow{k_{tH}} N_H(0) + Q(r)$
transfer to monomer	$N(r) + M \xrightarrow{k_{tM}} N(1) + Q(r)$
reinitiation by monomer	$N_H(0) + M \xrightarrow{k_H} N(1)$
	$N_A(0) + M \xrightarrow{k_A} N(1)$
	$N_S(0) + M \xrightarrow{k_S} N(1)$
spontaneous deactivation	$N(r) \xrightarrow{k_{ds}} N_d + Q(r)$

the mechanism. As a result, propagation reactions are assumed to be first order (rather than higher order) in ethylene.

The reaction mechanisms considered in this model, which are similar to those used in refs 7 and 23−26, are summarized in Table 2. Some less important reactions, e.g., reactions with various impurities and reinitiation by cocatalyst, are excluded from this model to achieve a simple, yet reasonable, reaction scheme. Since no long-chain branches were found in the product, using NMR analysis, reactions involving β-hydride elimination and subsequent insertion of macromonomers were also excluded from the mechanism. Also, since no internal or terminal double bonds were observed by NMR, side reactions that might generate hydrogen were neglected in the mechanism. The symbols for all pertinent species are defined in the Nomenclature.

A single-site mathematical model for semibatch ethylene homopolymerization, based on the mechanisms in Table 2, is shown in Table 3. The model consists of a set of dynamic mass balances for all the species present in the reactor: potential active sites (N*), initial active sites (N(0)), dormant active sites ($N_H(0)$, $N_A(0)$, $N_S(0)$), living polymer of chain length r (N(r)), ethylene (M), hydrogen (H_2), and dead polymer (Q(r)). The number-average molecular weight (Mn), weight-average molecular weight (Mw), and polydispersity (PDI) are evaluated using the method of moments. In the material balances equations for ethylene and hydrogen in Table 3, M and H_2, on the left-hand sides of the respective balances, are the number of moles of ethylene and hydrogen, respectively, in the gas phase. $[M]_{amr}$ and $[H_2]_{amr}$ are the corresponding concentrations in the amorphous polymer phase, determined using Henry's law.[21] We assume that the total number of moles in the gas phase remains constant through each experimental run, because a mixture of ethylene and hydrogen is fed to the reactor to replace the ethylene and hydrogen consumed by reaction, maintaining a constant pressure. The molar ratio of hydrogen to ethylene in the feed was set at r_{HM}, so that the mole fraction of ethylene in the feed was $1/(1 + r_{HM})$.

There are 22 unknown kinetic parameters, including activation energies, which need to be estimated in the single-site ethylene homopolymerization model in Table 3. Parameters were estimated using the measured gas feed rates and compositions during each run and the average molecular weights and polydispersity for polymer removed from the reactor at the end of each run. Parameter estimates were determined using the GREG[27]

Table 3. Material Balance Equations on Activation Sites, Monomer, and Polymer Chains in Single-Site Model

Mass Balance on Potential Active Sites inside Reactor

$$dN^*/dt = -k_{fdc}N^*[A]$$

Mass Balance on Initial Active Sites inside Reactor

$$dN(0)/dt = k_{fdc}N^*[A] - \{k_i[M]_{amr} + k_{ds}\}N(0)$$

Mass Balance on Dormant Active Sites after Chain Transfer to Hydrogen

$$dN_H(0)/dt = k_{tH}Y_0[H_2]_{amr} - k_H[M]_{amr}N_H(0)$$

Mass Balance on Dormant Active Sites after Chain Transfer to MAO

$$dN_A(0)/dt = k_{tA}Y_0[A] - k_A[M]_{amr}N_A(0)$$

Mass Balance on Dormant Active Sites after Chain Transfer to Scavenger

$$dN_S(0)/dt = k_{tS}Y_0[S] - k_S[M]_{amr}N_S(0)$$

Mass Balances on Ethylene and Hydrogen

$$dM/dt = [1/(1 + r_{HM})]\{\{k_pY_0 + k_iN(0) + k_HN_H(0) + k_AN_A(0) + k_SN_S(0)\}[M]_{amr} + k_{tH}Y_0[H_2]_{amr}\} - k_pY_0 + k_iN(0) + k_HN_H(0) + k_AN_A(0) + k_SN_S(0)\}[M]_{amr}$$

$$dH_2/dt = [r_{HM}/(1 + r_{HM})]\{\{k_pY_0 + k_iN(0) + k_HN_H(0) + k_AN_A(0) + k_SN_S(0)\}[M]_{amr} + k_{tH}Y_0[H_2]_{amr}\} - k_{tH}Y_0[H_2]_{amr}$$

$$[M]_{amr} = h_{C2}P_{M.gas} = h_{C2}(MRT/V_{rxr})$$

$$[H_2]_{amr} = h_{H2}P_{H2.gas} = h_{H2}(H_2RT/V_{rxr})$$

$$h_{C2} = 10^{-2.38+1.08(282/temperature)^2}(1 + k_{hen})$$

$$h_{H2} = 10^{-2.38+1.08(235/temperature)^2}$$

Moments of Living Polymer Chain Length Distribution

Zeroth Moment

$$dY_0/dt = \{k_iN(0) + k_HN_H(0) + k_AN_A(0) + k_SN_S(0)\}[M]_{amr} - \{k_{tA}[A] + k_{tS}[S] + k_{tH}[H_2]_{amr} + k_{ds}\}Y_0$$

First Moment

$$dY_1/dt = \{k_pY_0 + k_iN(0) + k_HN_H(0) + k_AN_A(0) + k_SN_S(0)\}[M]_{amr} - \{k_{tA}[A] + k_{tS}[S] + k_{tH}[H_2]_{amr} + k_{ds}\}Y_1 - k_{tM}[M]_{amr}(Y_1 - Y_0)$$

Second Moment

$$dY_2/dt = k_p(2Y_1 + Y_0)[M]_{amr} + k_iN(0)[M]_{amr} + \{k_HN_H(0) + k_AN_A(0) + k_SN_S(0)\}[M]_{amr} - \{k_{tA}[A] + k_{tS}[S] + k_{tH}[H_2]_{amr} + k_{ds}\}Y_2 - k_{tM}[M]_{amr}(Y_2 - Y_0)$$

Moments of Dead Polymer Chain Length Distribution

Zeroth Moment

$$dX_0/dt = \{k_{tA}[A] + k_{tS}[S] + k_{tH}[H_2]_{amr} + k_{ds} + k_{tM}[M]_{amr}\}Y_0$$

First Moment

$$dX_1/dt = \{k_{tA}[A] + k_{tS}[S] + k_{tH}[H_2]_{amr} + k_{ds} + k_{tM}[M]_{amr}\}Y_1$$

Second Moment

$$dX_2/dt = \{k_{tA}[A] + k_{tS}[S] + k_{tH}[H_2]_{amr} + k_{ds} + k_{tM}[M]_{amr}\}Y_2$$

Number-Average Molecular Weight, Mn

$$Mn = 28(X_1 + Y_1)/(X_0 + Y_0)$$

Weight-Average Molecular Weight, Mw

$$Mw = 28(X_2 + Y_2)/(X_1 + Y_1)$$

Polydispersity

$$PDI = Mw/Mn$$

Hydrogen Mole Fraction

$$f_{H2} = H_2/(M + H_2)$$

multivariate nonlinear regression software, which is capable of handling a variety of response variables that are measured at different sampling times.[28] Estimating the parameters in this model was very difficult, because some parameters have very little influence on the model predictions, and the effects of some parameters are highly correlated with the effects of other parameters. As a result, parameter estimates are highly correlated, and multiple sets of parameter estimates can give nearly the same model predictions. Many efforts were made to reduce the correlation between parameter estimates and to improve the conditioning of the parameter estimation problem. For example, a centered Arrhenius equation[29] was used to reduce correlation. In addition, logarithmic transformations were used to ensure that all kinetic parameter estimates were positive (since negative values do not make physical sense).[15]

Although there are extensive publications on modeling of polyethylene processes, parameter estimates could not be obtained from the literature to serve as initial guesses in the current model. Since obtaining parameter estimates using experimental data takes much more time and resources than the development of the model equations, most modelers only build models to obtain qualitative predictions and do not estimate parameters in the model with experimental data. They usually use arbitrary parameter values to simulate polymerization.[1−6] Unfortunately, the few publications with parameter estimates do not apply to current research. So far, the most similar work was done by Chakravarti and Ray[30] and Chakravarti et al.,[31] who did not divulge the structure of their catalyst or how it was supported. They also used rate constant units expressed per mass of catalyst, presumably including the support, making it impossible to convert their rate constants into values that could be used in our current modeling efforts

In the current research, the initial guesses were obtained in the following ways:

(a) For most important parameters, e.g. k_p, hand calculations were used to obtain order of magnitude values for the parameter.

(b) Models with simpler mechanisms were developed and fitted to obtain rough ranges for physically important parameters, e.g. k_p and k_{tS}.

(c) Activation energies were harder to guess than reference rate constants. For important parameters, e.g. k_p and k_{tS}, corresponding initial activation energies were obtained by fitting the simpler model. If no reasonable parameter estimates could be obtained, e.g. Ea_{kH}, and Ea_{ktH}, a rule of thumb value of 70000 J/mol was used as the initial guess, which means that the rate doubles with every 10 °C temperature increase. For parameters considered less important, based on physical understanding of ethylene polymerization and data analysis,[14] e.g. k_{tA} and k_{tM}, the corresponding activation energies were initially set to the lower boundary imposed for all activation energies that was used by GREG, i.e. 1000 J/mol, because the effect of temperature on these rate constants may not be able to be estimated from the available experimental data.

An estimability analysis,[12] which accounts for correlation among the effects of the parameters, was used to rank the parameters from most easily estimated to most difficult and to determine subsets of parameters that could be estimated together using the available data. A brief description of the estimability analysis algorithm is presented in Appendix A. An iterative parameter estimation scheme, which involves performing estimability analysis during nonlinear regression and dividing parameters into a series of subsets of estimable parameters, was used because attempts to estimate the complete set of parameters failed.

Table 4. Parameter Estimates in the Single-Site Homopolymerization Model

parameter	initial value[a]	parameter estimate 1	half-width of 95% HPD interval[b]
		Subset 1	
Ea_{kds}	11.896	12.542	0.012
Ea_{kS}	12.235	12.232	0.055
$k_{p.ref}$	10.309	11.048	0.021
Ea_{kH}	11.156	11.869	0.028
$k_{tH.ref}$	11.513	12.270	0.059
$k_{tS.ref}$	6.908	7.149	0.048
Ea_{ktS}	11.603	11.620	0.075
$k_{tA.ref}$	4.605	7.643	0.031
		Subset 2	
Ea_{kp}	10.322	10.397	0.039
$k_{S.ref}$	−1.204	−1.197	0.028
$k_{H.ref}$	4.605	5.983	0.049
$k_{ds.ref}$	−6.908	−8.717	0.038
$k_{i.ref}$	2.303	1.595	0.177
Ea_{kA}	11.156	11.490	0.162
Ea_{ktH}	11.156	10.093	0.149
$k_{A.ref}$	4.605	4.504	0.172
$k_{fdc.ref}$	8.517	6.979	0.182
		Unestimatable	
Ea_{kfdc}	6.908	6.908	
Ea_{ki}	6.908	6.908	
$k_{tM.ref}$	−27.631	−27.631	
Ea_{ktM}	6.908	6.908	
Ea_{ktA}	6.908	6.908	

[a] All parameters are transformed by taking the natural logarithm. [b] The half-widths of 95% HPD intervals are also based on transformed parameters.

The initial values, point estimates, and 95% confidence intervals for the parameters that were estimated are reported in Table 4. Note that the parameter estimates, confidence intervals and correlation matrices reported in this study were obtained using natural logarithm transformations of the parameters. For example, the logarithm-transformed point estimate for E_{akds} in Table 4 is 12.542, which corresponds to $e^{12.542}$ or 279850 J/mol. To estimate the parameters, first the most easily estimated parameters (8 parameters in subset 1) were estimated, while keeping all other parameter values at their initial guesses. Next, the values of the parameters in subset 1 were fixed, and another subset of 9 estimable parameters was estimated. After two subsets of parameters were estimated, no more parameters were found estimable based on estimability analysis of the remaining parameters. Using this technique, 17 out of the 22 unknown parameters were estimated using the data.

Five parameters, Ea_{kfdc}, Ea_{ki}, $k_{tM.ref}$, Ea_{ktM}, and Ea_{ktA}, were not estimable using an estimated cutoff criterion.[15] Two of them are associated with chain transfer to monomer, which indicates that chain transfer to monomer did not appear to have an important influence on the measured responses. Either the current measurements do not contain information about this reaction due to the types of experiments that were performed, or chain transfer to monomer does not occur to an appreciable extent. It is also noted that all four unestimable activation energies remained at their lower boundaries (the initial guesses) because there was not enough information in the data to reveal the effect of

temperature on these reactions. Since the results of an estimability analysis depend on the parameter values used to determine the sensitivity coefficients, different initial guesses were also tested to make sure that the unestimability of some parameters did not result from the selection of poor initial guesses. New initial values were deliberately chosen to enhance the parametric sensitivities for the five unestimable parameters in an effort to make them become estimable. With most initial guesses, these parameters became unestimable after several iterations of the nonlinear regression. In some cases, the number of unestimable parameters was less than five and one or two of these five parameters, e.g. Ea_{ki}, remained estimable at the end of regression. However, estimability analysis using the revised initial parameter estimates showed that these five parameters still stayed close to the bottom of rank of the estimability analysis, indicating that they were not influential in the model predictions for the 11 experimental runs.

In addition to point estimates for the transformed parameters, Table 4 also shows the interval estimates, which are expressed as half-widths of 95% HPD (highest posterior density) intervals. In each subset of estimable parameters, parameters are listed according to their rank from the estimability analysis. By comparing the half-width of 95% HPD intervals of parameters in the same subset, it appears that the interval estimates are consistent with the estimability analysis. A parameter that ranked higher in the estimability analysis usually has a smaller uncertainty interval. The comparison between interval estimates from the first and second subsets also reveals that interval estimates in the first subset have narrower half-widths of 95% HPD intervals than those in the second subset of estimable parameters, presumably because there is more information in the data set about the first set of estimable parameters.

The correlation matrices[15] for the two subsets of estimated parameters revealed that some correlations between reference rate constants and activation energies are still very high, even though a centered Arrhenius equation was used. Most reference rate constants were not in the same subset with their corresponding activation energy. k_{tS} and k_A are the only parameters having both reference rate constant and activation energy in the same subset, and their respective correlation coefficients are 0.73 and 0.74, respectively. It was also apparent that the parameters associated with chain transfer and the corresponding reinitiation reaction tend to have strong correlations. For example, the correlation is -0.71 between $k_{tH.ref}$ and Ea_{kH}, 0.71 between $k_{tS.ref}$ and Ea_{kS}, and 0.98 between Ea_{kS} and Ea_{ktS}. The generation of active sites is controlled by two cascade reactions, i.e. active site formation and initiation. The correlation between the corresponding parameters in this cascade is also high, as indicated by the -0.83 correlation coefficient between $k_{fdc.ref}$ and $k_{i.ref}$.

Using the parameter estimates in Table 4, model predictions of ethylene feed rate, hydrogen concentration, and molecular weight are compared with experimental data in Figures 2−4, respectively. The error bars in Figures 3 and 4 are the 95% confidence intervals for the experimental data, which were obtained from four replicate ethylene−hexene copolymerization runs conducted using the same catalyst and reactor system. To avoid clutter, error bars are not shown for the numerous ethylene feed rate measurement points in Figure 1.

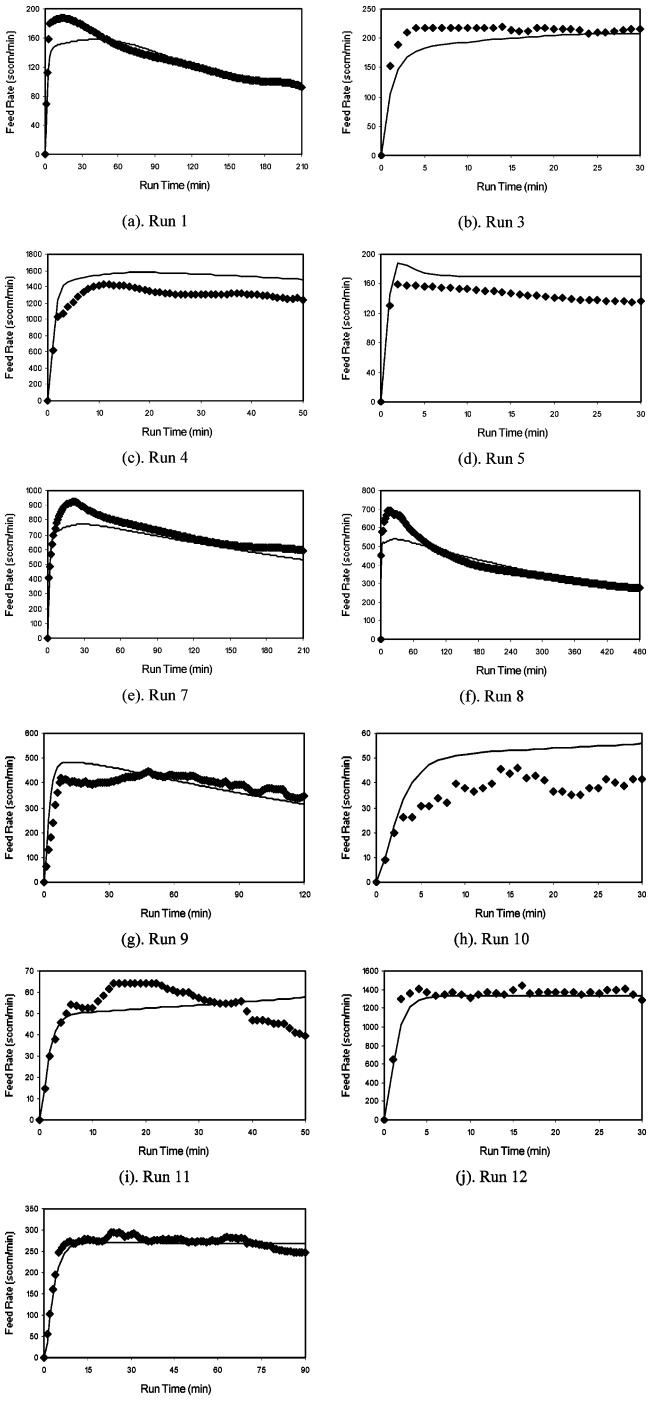

Figure 2. Experimental data and model predictions of ethylene feed rate (the lines are model predictions, and the diamonds are experimental data points).

Approximate 95% confidence intervals for the measured ethylene feed rates are at ±44% of the measured values.

Figure 2 shows that the single-site model can predict most ethylene feed rate data well, especially when the widely differing rate scales of the graphs in Figure 2 are taken into consideration. Most model predictions are close to their experimental data. However, it appears that the model cannot always predict the rate peak in the early stage of polymerization very well. If there is no large peak at the beginning of polymerization, as in runs 3, 4, 5, 9, 10, 11, and 13, model predictions match the experimental data better than in runs 1, 7, and 8, where there is a larger peak during the early stage of

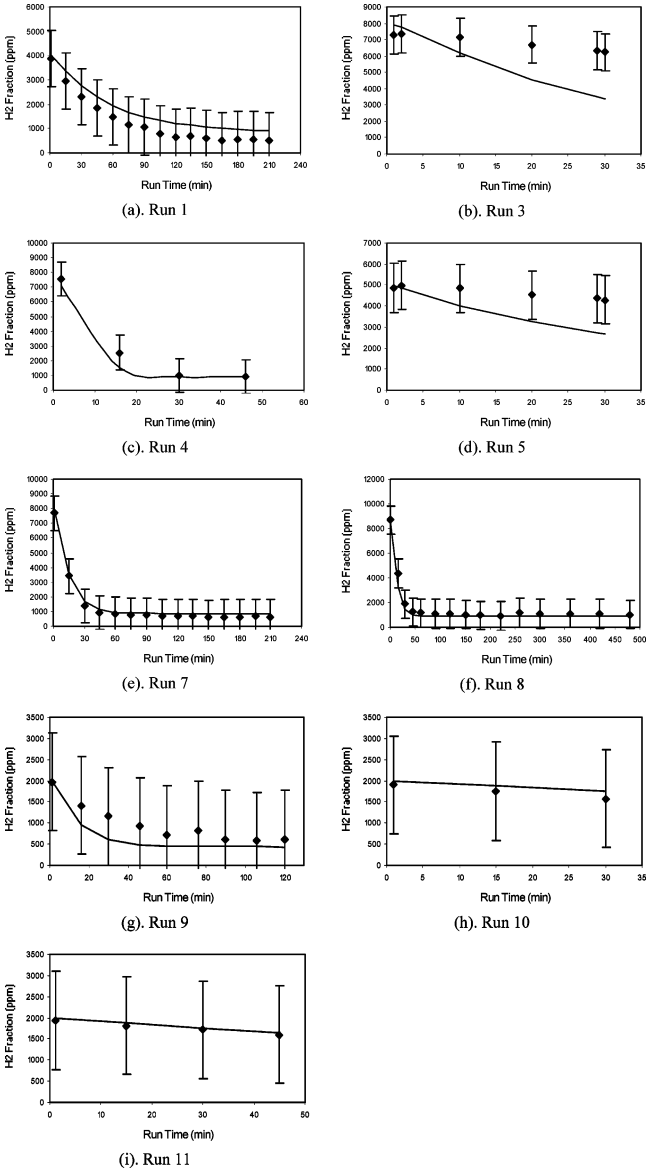

Figure 3. Experimental data and model predictions of hydrogen concentration (the lines are model predictions, and the diamonds are experimental data points).

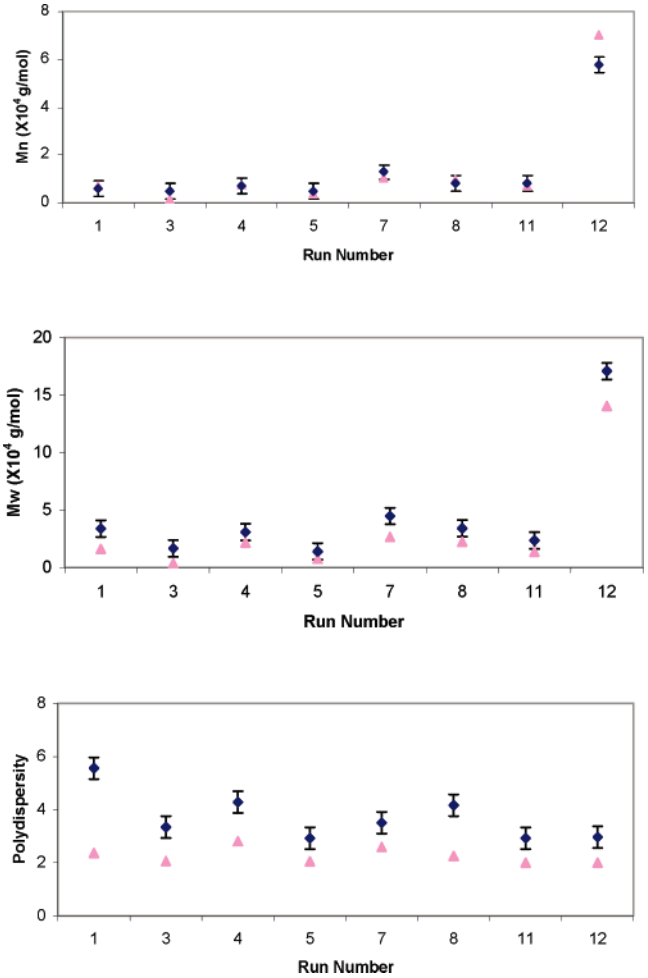

Figure 4. Experimental data and model predictions of molecular weight (the triangles are model predictions, and the diamonds are experimental data points).

polymerization. When there is an initial large peak, the model tends to underpredict the ethylene feed rate during the first 10−30 min.

In Figure 3, the single-site model fits the hydrogen concentration data well. Except for the final three data points in runs 3 and 5, all model predictions fall into the 95% confidence intervals of the experimental data. However, Figure 4 shows strong lack of fit for the molecular weight data. The single-site model mostly predicts number-average molecular weight (Mn) within the 95% confidence intervals, only failing to accurately predict the Mn observation in runs 3, 7, and 12. However, for weight-average molecular weight, all eight model predictions are well below their experimental values and are outside of the 95% confidence intervals. For polydispersity, all model predictions are close to 2 and are significantly below the experimental observations. This result was disappointing. Although we recognized that the single-site model would always predict polydispersities near 2 if the gas composition were constant during each run, we had anticipated that the higher measured polydispersities might be explained by polymer with different average instantaneous molecular weights being produced at different times during each run, due to gas composition drift. Several attempts have been made to improve the model predictions of molecular weight data, especially the polydispersity predictions.

(a) Numerous initial parameter guesses were used to find better fits, but no significant improvement was observed using the single-site homopolymerization model.

(b) In the experimental data, there are over 1000 rate observations, but only ~30 molecular weight observations for Mn, Mw, or PDI. Therefore, the poor fitting of molecular weight might have been caused by the relatively small focus of the parameter estimation algorithm on obtaining small residuals for the limited number of molecular weight predictions. Weighted least squares was tried to seek improvement in model predictions of molecular weight. However, very little improvement was achieved even with very large penalties on molecular weight residuals. The predicted PDI was always below 3, compared to a range from 2.9 to 5.6 for the experimental data.

(c) While assuming only a single type of active site, different mechanisms were tried to obtain better fitting of molecular weight, including β-hydride elimination and reactions with impurities. However, no improvement was observed.

As a result, the lack of fit appears to be caused by an inadequate model mechanism, rather than the parameter estimation methodology. According to mathematical models and mechanism studies in the literature, there are three options to modify the model mechanism in the current model:

(a) Incorporate more reactions at the single type of site. The chemical reactions considered in the current model are still simpler than some complex models.[1,2] More reactions, such as reactions with different orders for deactivation, could be added to the model. However, unless the additional mechanisms would cause a significant change in instantaneous molecular weight at different stages of polymerization, the accumulated molecular weight distribution would still have a predicted PDI near 2.

(b) Incorporate heat- and mass-transfer resistances in the model. Models that consider mass- and heat-transfer resistances can result in polydispersity predictions corresponding to broader molecular weight distributions.[32] However, this approach would not be helpful for the catalyst used in the current research, because, according to the criteria established by Floyd et al.,[16−20] heat- and mass-transfer resistances should not be significant contributors to broad molecular weight distributions, since the activity of the metallocene catalyst used in this work was too low to result in significant heat- and mass-transfer resistances.

(c) Incorporate two or more types of catalyst sites. When there is more than one type of active site, the overall instantaneous molecular weight distribution will be the weighted sum of several Flory most probable distributions, which, in turn, results in broader molecular weight distribution.

Based on the vast reports on catalyst heterogeneity in the literature, especially for supported catalysts, it is believed that multiple active site types are mainly responsible for the broad molecular weight distributions observed in low-pressure olefin polymerization. Therefore, a two-site model was developed to describe the model mechanism and to improve model predictions.

Two-Site Model

Physical Explanation of Heterogeneity in Supported Metallocene. Although a few researchers have shown evidence of multiple site types in homogeneous reaction environments,[33] unsupported metallocenes are usually considered to be single-site catalysts. However, significant site heterogeneity in supported metallocenes has been reported. The effects of the support on polymerization behavior and product properties have been widely studied. It has been found that the supported metallocenes may not only show lower catalyst activity in ethylene polymerization[34−37] compared with unsupported metallocenes but can also lead to larger polydispersities.[35,36,38−40]

Sacchi et al.[35] studied ethylene polymerization with Cp_2ZrCl_2, a catalyst similar to that used in the current research. They found that the unsupported metallocene showed homogeneous behavior, including a narrow molecular weight distribution. However, when the metallocene was supported on silica, the polydispersity ranged from 2.9 to 7.9, which is an even larger range than the polydispersities from the current experiments.

Chu et al.[36,40] studied ethylene homopolymerization and ethylene/1-hexene copolymerization with homogeneous, supported, and self-supported $Et[Ind]_2ZrCl_2$.

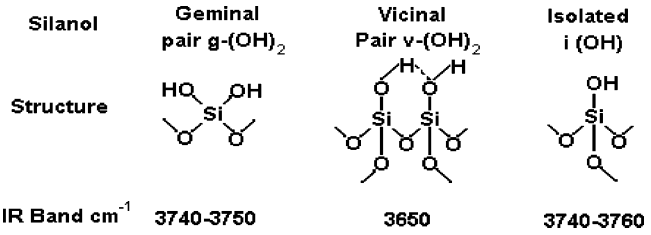

Figure 5. Hydroxyl groups on silica.

Catalyst activity was lower for the supported catalysts, and the molecular weight distributions were broader (2.1−2.6 for unsupported vs 2.6−3.1 for supported).

Kumkaew et al.[41] used temperature rising elution fractionation (TREF), differential scanning calorimetry (DSC), and size exclusion chromatography (SEC) to analyze polyethylene made with supported $(n\text{-BuCp})_2ZrCl_2$. The study of support pore sizes showed that these catalysts contained multiple types of catalytic sites and the support pore size had strong effects on the types of sites.

The heterogeneity of supported metallocene catalysts can be caused by the heterogeneity of the silica support, as well as the supporting process. When metallocene is supported on silica, the catalyst molecules are immobilized by chemical reactions with the surface hydroxyl groups on the silica.

$$(BuCp)_2ZrCl_2 + HO{-}Si{\equiv} \rightarrow (BuCp)_2Zr(Cl){-}O{-}Si{\equiv} + HCl$$

As shown in Figure 5, there are three kinds of hydroxyl groups in silica, geminal pairs g-$(OH)_2$, vicinal pairs v-$(OH)_2$, and isolated i-(OH). They absorb at different wavelengths in the IR spectrum.[42,43] Therefore, when metallocenes react with different hydroxyl groups, the immobilized catalyst sites are immobilized in different environments and may show different catalytic behavior during ethylene polymerization.

Another possible cause of multiple types of active sites is the existence of free catalyst molecules that are physically rather than chemically adsorbed onto the catalyst support. During the catalyst supporting process, catalysts are either chemically bonded to the silica or physically adsorbed on the surface, which may introduce two types of active sites. The physically adsorbed catalyst molecules can be distributed on the inner surfaces of the pores or the outer surface of particles. After supporting, the catalysts are usually filtered and washed with solvent. The filtration of catalysts can remove the free catalysts that are neither physically nor chemically attached to the support. The catalysts physically adsorbed on the outer surface of the support can be removed by washing with solvent. However, the free catalysts adsorbed on the inner surface may be difficult to remove. Therefore, even after filtering and washing, there may still exist two kinds of active sites on the support, which may exhibit different catalytic behavior during polymerization and may produce broad molecular weight distributions if their ratios of propagation rate to chain transfer rates are very different.

Examination of the molecular weight distribution (MWD) curves also indicates the possibility of multiple active sites. Figure 6 shows the MWD curves from four runs. The pronounced shoulders in the MWD curves for runs 1 and 3 suggest that there are multiple active site types. The flat peak tops in runs 2 and 5 may also be

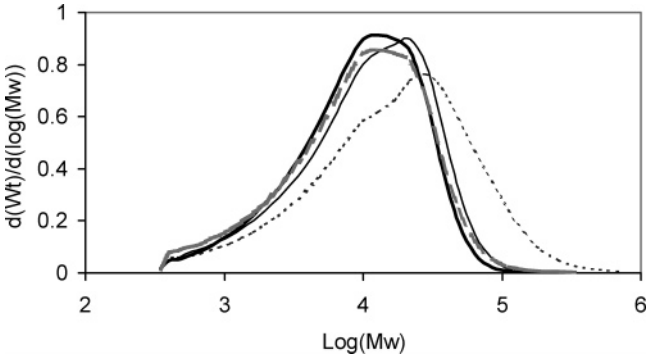

Figure 6. Molecular weight distribution from homopolymerization products (dotted line, run 1; dashed line, run 2; thin solid line, run 3; thick solid line, run 5)

Table 5. Reaction Mechanisms of the Two-Site Homopolymerization Model

active sites formation	$N_1^* + A \xrightarrow{k_{FDC}} N_1(0)$
	$N_2^* + A \xrightarrow{k_{FDC}} N_2(0)$
active sites initiation	$N_1(0) + M \xrightarrow{k_i} N_1(1)$
	$N_2(0) + M \xrightarrow{k_i} N_2(1)$
propagation	$N_1(r) + M \xrightarrow{k_{P1}} N_1(r+1)$
	$N_2(r) + M \xrightarrow{k_{P2}} N_2(r+1)$
transfer to cocatalyst	$N_1(r) + A \xrightarrow{k_{tA}} N_{A1}(0) + Q(r)$
	$N_2(r) + A \xrightarrow{k_{tA}} N_{A2}(0) + Q(r)$
transfer to scavenger	$N_1(r) + S \xrightarrow{k_{tS}} N_{S1}(0) + Q(r)$
	$N_2(r) + S \xrightarrow{k_{tS}} N_{S2}(0) + Q(r)$
transfer to hydrogen	$N_1(r) + H_2 \xrightarrow{k_{tH}} N_{H1}(0) + Q(r)$
	$N_2(r) + H_2 \xrightarrow{k_{tH}} N_{H2}(0) + Q(r)$
transfer to monomer	$N_1(r) + M \xrightarrow{k_{tM}} N_1(1) + Q(r)$
	$N_2(r) + M \xrightarrow{k_{tM}} N_2(1) + Q(r)$
reinitiation by monomer	$N_{H1}(0) + M \xrightarrow{k_H} N_1(1)$
	$N_{H2}(0) + M \xrightarrow{k_H} N_2(1)$
	$N_{A1}(0) + M \xrightarrow{k_A} N_1(1)$
	$N_{A2}(0) + M \xrightarrow{k_A} N_2(1)$
	$N_{S1}(0) + M \xrightarrow{k_S} N_1(1)$
	$N_{S2}(0) + M \xrightarrow{k_S} N_2(1)$
spontaneous deactivation	$N_1(r) \xrightarrow{k_{ds}} N_d + Q(r)$
	$N_2(r) \xrightarrow{k_{ds}} N_d + Q(r)$

caused by the overlap of two or more peaks from different types of active sites.

Development of the Two-Site Model. Because of the apparent existence of multiple types of active sites and unsatisfactory fitting of molecular weight using the single-site model, a two-site model was developed. In a full two-site model, the number of unknown parameters would almost double if different rates were assumed for all types of reactions shown in Table 5. Since it was impossible to estimate all the unknown parameters in the single-site model, using the same data set to fit a full two-site model would exacerbate this problem. Therefore, a simplifying assumption was made that leads to a two-site model with only a few extra parameters.

The major problems identified in the single-site model predictions were in fitting the peak rates during the initial stages of polymerization and the average molecular weights and polydispersities. Since molecular weights and polydispersities mainly depend on the ratio of the propagation rate to the rate of transfer to hydrogen at the two types of sites, having different ratios of these parameters for different sites will lead to larger polydispersities. If the two sites had the same propagation rate constant but different rate constants for chain transfer to hydrogen, then larger polydispersities would be predicted. However, the reaction rate behavior would not be significantly affected. Since both the polydispersity and the reaction rate behavior are influenced by the relative propagation rates at the two sites, different propagation rate constants were assumed for the two sites, while all other kinetic parameters were assumed to have common values for the two sites, to keep the number of additional parameters to estimate to a minimum.

If the two types of sites result from different types of interactions with the support, then both types of active sites will be present from the start of the polymerization, and the relative amounts of the two types of sites must be known in order to make predictions of reaction rates and product properties. As a result, the two-site model requires one additional propagation rate constant and an additional constant, which is the fraction of active sites, f_{c1}, that belong to the first site type. To account for the influence of temperature on the additional propagation rate constant, an activation energy for the new propagation rate constant was also included as a parameter in the two-site model. Therefore, this simplified two-site model has 25 unknown parameters, compared with 22 for the one-site model. The mechanism for the two-site model is listed in Table 5.

Parameter Estimation and Simulation Results: Two-Site Model. Parameter estimates from the single-site model were used as initial guesses for the two-site model except for $k_{p1.ref}$, Ea_{kp1}, $k_{p2.ref}$, Ea_{kp2}, and f_{c1}. f_{c1} was set to the middle of its range, i.e. 0.5. Active site type 1 was chosen as the more active site type, with the initial value for $k_{p1.ref}$ set 50% higher than the propagation parameter in the single-site model. Active site 2, the lower activity site, had an initial propagation rate constant, $k_{p2.ref}$, that was 50% lower than the estimate of $k_{p.ref}$ from the single-site model. The activation energies of propagation rate constants for both site types were initially set at the same value, at the corresponding parameter estimate from the single-site model. The initial guesses and parameter estimates are listed in Table 6. Parameter estimates were obtained using the same iterative method used for the single-site model.

Of the 25 unknown parameters, 22 parameters were found estimable and estimated as four subsets with 19, 1, 1, and 1 parameter, respectively. Three parameters, Ea_{ki}, $k_{tM.ref}$, and Ea_{ktM}, could not be estimated. These three unestimable parameters are also unestimable in the single-site homopolymerization model. The two other unestimable parameters in the single-site model were ranked in the final two subsets in the two-site model. Their confidence interval estimates, ± 6.117 and ± 1.971 for the logarithm-transformed parameters, are also the worst for all estimable parameters, giving a

Table 6. Parameter Estimates in the Two-Site Homopolymerization Model

parameter	initial value[a]	parameter estimate[a]	half-width of 95% HPD interval[b]
		Subset 1	
Ea_{kS}	12.232	12.304	0.086
$k_{pB.ref}$	10.355	11.696	0.058
Ea_{kH}	11.869	11.975	0.136
Ea_{kds}	12.542	11.795	0.726
f_{c1}	−0.693	−0.688	0.030
$k_{tS.ref}$	7.149	7.360	0.242
$k_{tA.ref}$	7.643	7.969	0.064
$k_{tH.ref}$	12.270	12.207	0.078
Ea_{ktS}	11.620	11.697	0.151
$k_{fdc.ref}$	6.979	6.807	0.189
Ea_{kA}	11.490	11.470	0.178
Ea_{kpB}	10.397	10.117	0.219
Ea_{kp1}	10.397	10.922	0.203
$k_{A.ref}$	4.504	4.703	0.200
$k_{S.ref}$	−1.197	−1.043	0.245
$k_{i.ref}$	1.595	1.729	0.236
$k_{H.ref}$	5.983	6.116	0.275
Ea_{ktH}	10.093	9.569	0.477
$k_{ds.ref}$	−8.717	−6.951	1.171
		Subset 2	
$k_{pA.ref}$	11.741	9.416	0.056
		Subset 3	
Ea_{ktA}	6.908	6.908	6.117
		Subset 4	
Ea_{kfdc}	6.908	6.908	1.971
		Unestimatable	
Ea_{ki}	6.908	6.908	
$k_{tM.ref}$	−27.631	−27.631	
Ea_{ktM}	6.908	6.908	

[a] All parameters are transformed by taking the natural logarithm. [b] The half-widths of 95% HPD intervals are also based on transformed parameters Ea_{ki}, $k_{tM.ref}$, and Ea_{ktM}.

strong indication of the lack of importance of these five parameters for obtaining accurate model predictions. Several sets of initial values were also tried, to study the effects of different initial values on the unestimability of these five parameters. Although some differences could be found in terms of the goodness of fit of the data, these five parameters appeared most frequently among the unestimable parameters.

Since Ea_{ki} could not be estimated in either the single- or two-site model, it seems that the data contain very little information about the effects of temperature on the rates of active site initiation. The unestimability of $k_{tm.ref}$ and Ea_{ktm} in both the single-site model and the two-site model indicates that chain transfer to monomer is not an important chain-stopping mechanism for the range of experimental conditions examined and points to the possibility of removing this reaction from the model mechanism.

The examination of interval estimates shows similar results as in the single-site model. A parameter that ranks higher in estimability analysis generally has a smaller confidence interval. The second subset consists of only one parameter, $k_{pA.ref}$, which is believed to be one of the most important parameters enabling us to obtain reasonable weight-average molecular weight and polydispersity predictions. Its large correlation with the other three parameters associated with propagation, i.e. $k_{pB.ref}$, Ea_{kpA}, and Ea_{kpB}, appears to be responsible for the low rank of $k_{pA.ref}$ in estimability analysis.

The correlations[15] among parameter estimates are consistent with those from the single-site model, e.g. high correlation between $k_{tS.ref}$ and $Ea_{ktS.ref}$, $k_{A.ref}$ and $Ea_{kA.ref}$, $k_{tS.ref}$ and Ea_{kS}, Ea_{kS} and Ea_{ktS}, etc. In the two-site model, the correlation between the reference rate constant and its corresponding activation energy is still strongest, e.g. −1.0 between $k_{ds.ref}$ and Ea_{kds} and 0.78 between $k_{tS.ref}$ and Ea_{ktS}. The correlation between parameters associated with chain transfer and subsequent reinitiation is also significant, e.g. 0.80 between Ea_{kS} and $k_{tS.ref}$ and 0.96 between $k_{S.ref}$ and $k_{tS.ref}$.

Using the parameter estimates in Table 6, the model predictions of ethylene feed rate, hydrogen concentration, and molecular weight are compared with experi-

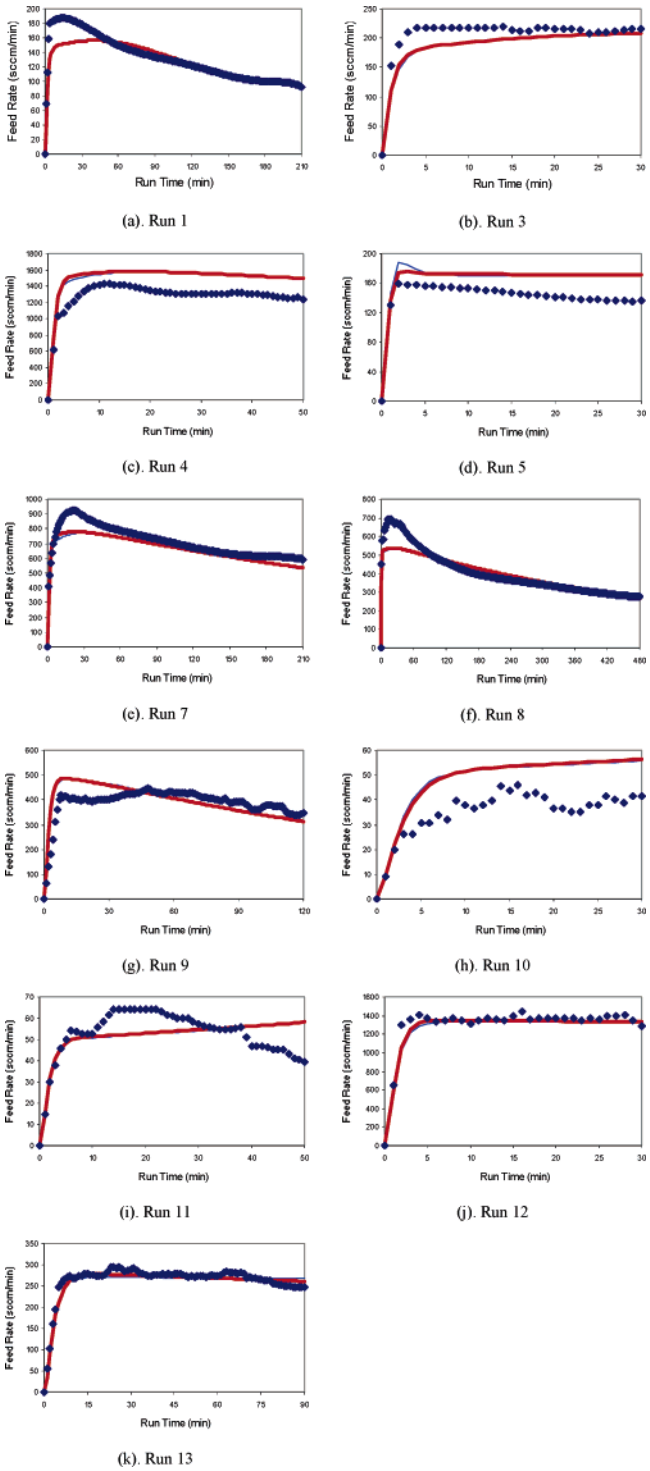

Figure 7. Experimental data and model prediction of ethylene feed rate (the thick lines are predictions from the two-site model, the thin lines are predictions from the single-site model, and the diamonds are experimental data points).

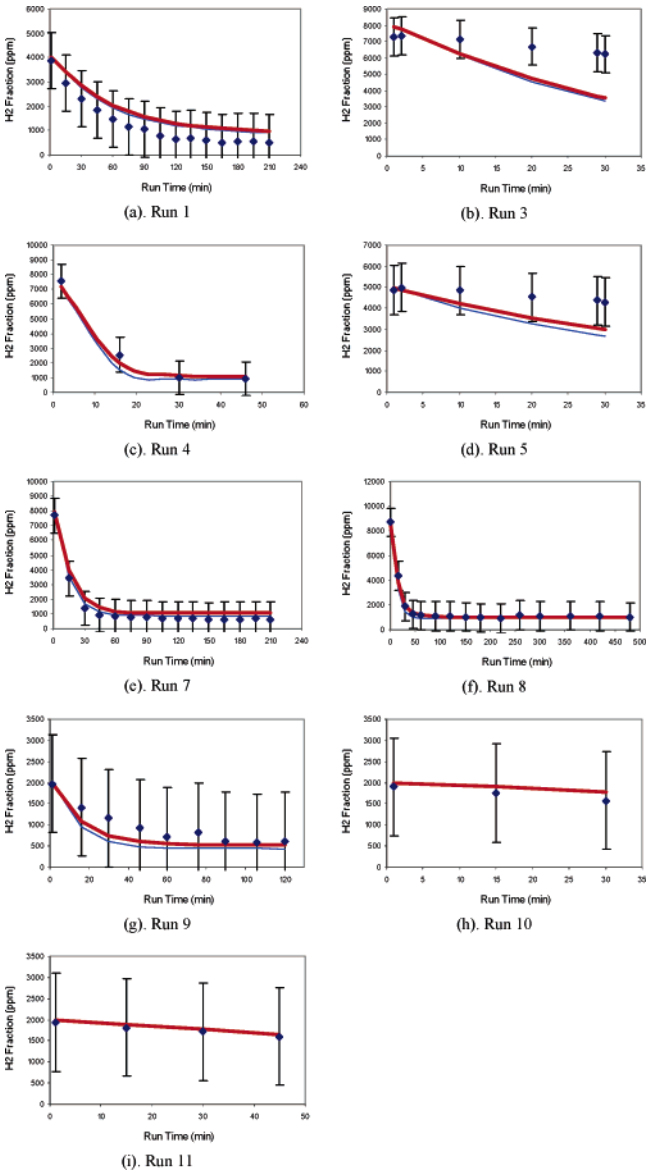

Figure 8. Experimental data and model prediction of hydrogen concentration (the thick lines are predictions from the two-site model, the thin lines are predictions from the single-site model, and the diamonds are experimental data points).

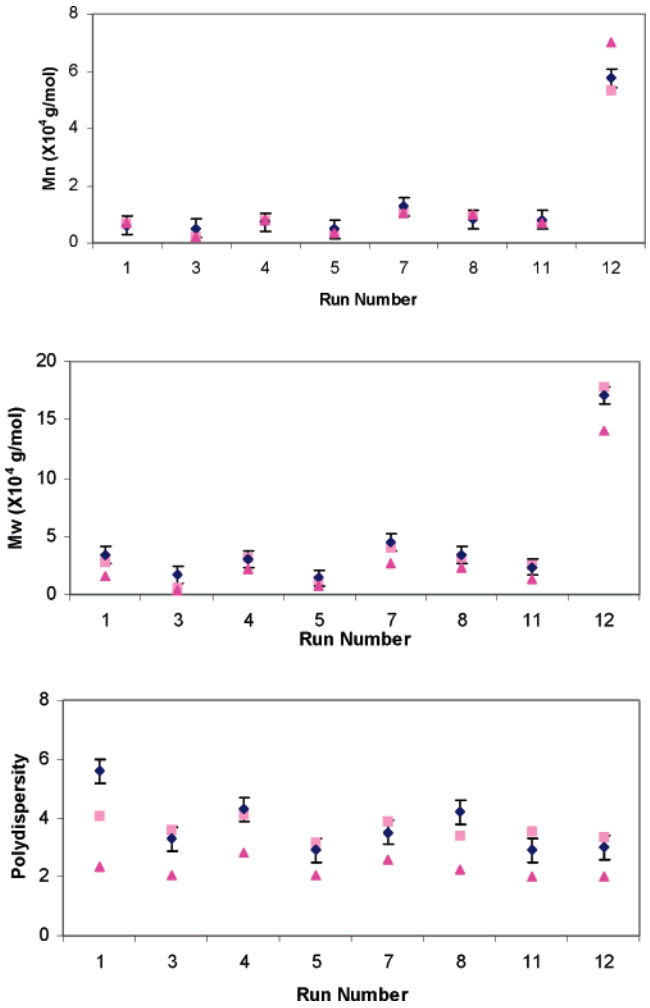

Figure 9. Experimental data and model prediction of molecular weight (the triangles are single-site model predictions, the squares are two-site model predictions, and the diamonds are experimental data points).

mental data in Figures 7−9, respectively. The error bars in Figures 8 and 9 show the 95% confidence intervals for the experimental data.

Figure 7 shows almost identical fitting of polymerization rate using the single-site model and the two-site model. The model predictions of the single-site model and the two-site model almost overlap with each other in all 11 runs. In runs with peaks during the initial stage, neither model can predict the peak very well. As shown in Figure 8, there is little, if any, improvement in the fit of the hydrogen concentrations. The two-site model gives better predictions in runs 3, 4, 5, and 9, but the single-site model matches the data slightly better in runs 1 and 7.

The two-site model shows significant improvement in fitting the molecular weight data, especially Mw and PDI. Using the two-site model, all model predictions fall between the 95% confidence intervals for the experimental molecular weight data, except for the Mw prediction in run 3. For polydispersity, none of the predictions from the single-site model fell into the 95% confidence intervals of experimental data, whereas, using the two-site model, five of eight predictions are inside of the 95% confidence intervals. These three two-site model predictions that are outside of the confidence intervals are much closer to the experimental data than the predictions from the single-site models.

With three extra parameters, the two-site model gives much better predictions of molecular weight properties. Although there are still some qualitative differences in the shapes of some of the polymerization rate curves, indicated by poor fitting of peak rates in the early stage of polymerization, the model can fit most of the rate data very well.

Model Verification

Using the two-site model and the parameter estimates obtained from the 11 homopolymerization runs, model predictions for runs 2 and 6 are shown in Figures 10 and 11 and Table 7. Figures 10 and 11 indicate that the model is able to predict both the polymerization rate and the hydrogen concentration very well. Note that run 2 resulted in a polymerization rate that is approximately 10 times lower than the polymerization rate in run 6, and the model predicts a 10-fold difference in the two rates. One of the major challenges in gas-phase ethylene polymerization is to obtain good reproducibility of

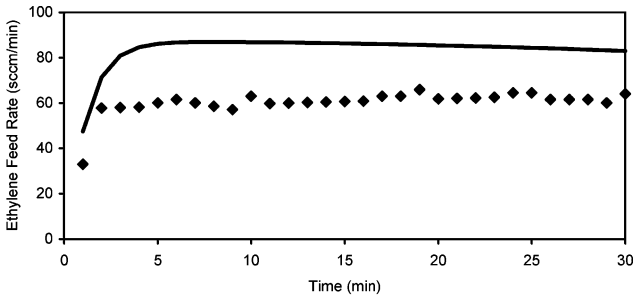

(a). Experimental data and model prediction of ethylene feed rate in Run 2

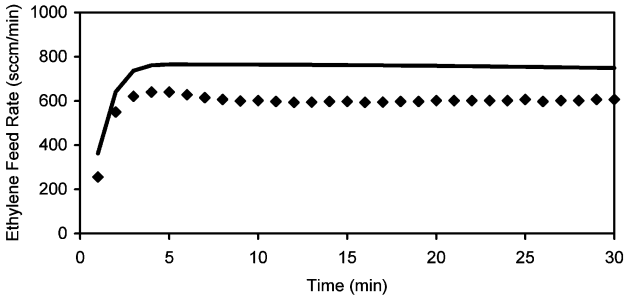

(b). Experimental data and model prediction of ethylene feed rate in Run 6

Figure 10. Model verification with ethylene feed rate (the lines are model predictions, and the diamonds are experimental data points).

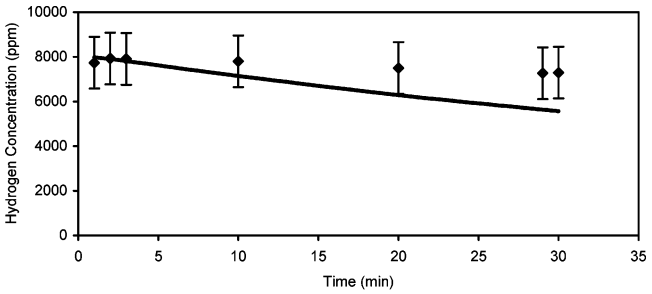

Experimental data and model prediction of hydrogen concentration in Run 2

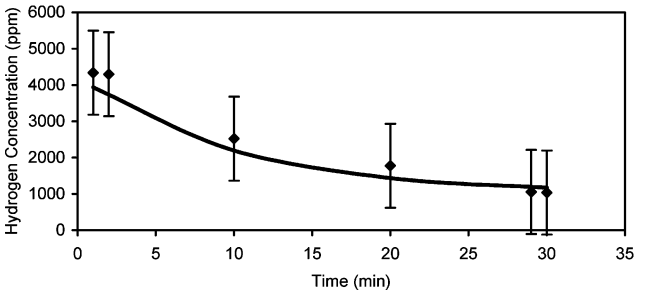

Experimental data and model prediction of hydrogen concentration in Run 6

Figure 11. Model verification with hydrogen concentration (the lines are model predictions, and the diamonds are experimental data points).

polymerization rate; we were only able to reproduce our rate data with a standard deviation of ±13.8%.[15] Therefore, predictions of the polymerization rate data were within the 95% confidence intervals of the experimental data.

All model predictions of the hydrogen concentration are within the 95% confidence intervals, except for the last two values for run 2, which are just outside of the interval. Table 7 shows that the model is also able to predict the molecular weight data quite well. The Mn and Mw predictions for run 6 are within the 95% confidence intervals, as are the Mn and PDI predictions for run 2. The predicted weight-average molecular weight for run 2, however, is lower than the measured value, falling outside of the 95% confidence interval. Since the measured molecular weight is so low, it is difficult to assess whether the mismatch results from an inaccurate model prediction or from an inaccurate molecular weight measurement. The confidence intervals for the molecular weight responses were determined using replicate runs for a polymer with a significantly higher molecular weight (weight-average molecular weight of approximately 25000 g/mol) and may not be valid for runs that produce polymers with very low molecular weights, which are difficult to measure accurately using high-temperature GPC. The PDI prediction in run 6 is also lower than experimental data and falls outside the 95% confidence interval, but the difference is not very large.

Table 7. Model Verification of Molecular Weight Data

	Mn		Mw		PDI	
run	expt	model	expt	model	expt	model
2	4400	1802	15300	6309	3.48	3.50
6	6800	7782	26800	26523	3.94	3.41
95% conf intvl	*±3197*		*±7202*		*±0.41*	

Conclusions

A single-site model was developed to simulate gas-phase ethylene homopolymerization using a supported metallocene catalyst. Measurements from 11 experimental runs were used to estimate the model parameters. Of 22 unknown parameters, 17 were found to be estimable using an iterative procedure. Two unestimable parameters are associated with chain transfer to monomer, indicating that chain transfer to monomer did not have an important influence on predictions of the measured responses. Either the current measurements do not contain enough information about these reactions due to the types of experiments that were performed, or they do not occur to an appreciable extent.

The single-site model provided plausible fits for both the polymerization rate and hydrogen concentration. However, it could not predict the molecular weight data very well, especially polydispersity. A simplified two-site model, with only three additional parameters, was developed to improve the model predictions. The two-site model showed significant improvements in the prediction of molecular weight and its distribution over the single-site model. Two extra experimental runs, whose data were not used in the parameter estimation process, were employed to validate the two-site model. Nearly all of the model predictions were within the 95% confidence intervals for the experimental polymerization, gas composition, and molecular weight data. This model should be a useful tool to predict the effects of operating conditions on gas-phase ethylene polymerization and to solve problems that may be met in the scale-up from lab-scale processes to commercial-scale processes.

Acknowledgment

The authors thank BP Chemicals for financial support of this research and for conducting GPC analyses.

Appendix A: Procedure of Estimability Analysis

Yao et al.[12] studied the parameter estimability of an ethylene/butene copolymerization model. They proposed a new method to rank parameters according to their estimability. This method is based on the analysis of sensitivity coefficients, which are the first-order partial derivatives of response variables, η_r, that are predicted by the model, with respect to the parameters at the particular times when the measurements are available.

$$\text{sensitivity coefficient} = \left.\frac{\partial \eta_r}{\partial \theta_p}\right|_{t_n}$$

First, a sensitivity coefficient matrix, Z, was formed from the individual sensitivity coefficients as follows:

$$Z = \begin{bmatrix} \left.\frac{\partial \eta_1}{\partial \theta_1}\right|_{t=t_1} & \cdots & \left.\frac{\partial \eta_1}{\partial \theta_P}\right|_{t=t_1} \\ \vdots & \ddots & \vdots \\ \left.\frac{\partial \eta_R}{\partial \theta_1}\right|_{t=t_1} & \cdots & \left.\frac{\partial \eta_1}{\partial \theta_P}\right|_{t=t_1} \\ \left.\frac{\partial \eta_1}{\partial \theta_1}\right|_{t=t_2} & \cdots & \left.\frac{\partial \eta_1}{\partial \theta_P}\right|_{t=t_2} \\ \vdots & \ddots & \vdots \\ \left.\frac{\partial \eta_R}{\partial \theta_1}\right|_{t=t_N} & \cdots & \left.\frac{\partial \eta_R}{\partial \theta_P}\right|_{t=t_N} \end{bmatrix}$$

where each column contains derivatives with respect to a particular model parameter, and each row contains derivatives for a particular response variable at a particular sampling time. In general, this sensitivity matrix will have many rows, one for each type of measured response, at each time that response is measured, for each experimental run.

To effectively compare coefficients, Yao et al.[12] used the following procedure to scale sensitivity coefficients:

$$\frac{\hat{\theta}_p}{\hat{\eta}_r|_{t_n}} \left.\frac{\partial \eta_r}{\partial \theta_p}\right|_{t_n}$$

where $\hat{\theta}_p$ is either an initial guess or a current parameter estimate and $\hat{\eta}_r|_{t_n}$ is the value of the rth predicted response variable at time t_n. This scaling was performed prior to any sensitivity or estimability calculations. $\hat{\theta}_p$ and $\hat{\eta}_r|_{t_n}$ were used for scaling because they reflect the approximate magnitudes of changes in parameter estimates and model predictions, respectively, during the parameter fitting procedure.

Two features govern the estimability of a parameter:[13] (1) the strong influence of that parameter on one or more of the measured responses and (2) the correlation between the effects of that parameter on model predictions and the corresponding effects of all other estimable parameters.

The first feature can be determined by examining the magnitude of each column of Z, which corresponds to a particular parameter. Columns of the sensitivity matrix with large magnitudes indicate that the particular parameter has a large effect on the predicted responses. The second feature demands that we examine whether the columns corresponding to the set of estimable parameters are correlated with each other. Theoretically, the column rank of the Z matrix is equal to the number of estimable parameters. But in the case where the rank is less than the number of columns, this rank assessment does not answer the question: which subsets of parameters could be estimated? Yao et al.[12] proposed the following procedure, which takes both features into account, to rank parameters according to their estimability. This ranking method was adopted in this paper.

1. Calculate the magnitude of each column of Z. Note that initial guesses for the parameter values are required to determine the elements of Z.
2. Pick the parameter whose column in Z has the largest magnitude as the first estimable parameter.
3. Mark the corresponding column as X_K ($K = 1$).
4. Calculate $\hat{Z}_K$, the least-squares prediction of the full sensitivity matrix, Z, obtained using the subset of columns, X_K: $\hat{Z}_K = X_K(X_K^T X_K)^{-1} X_K^T Z$.
5. Calculate the residual matrix R_K: $R_K = Z - \hat{Z}$.
6. Calculate the magnitude of each column of R_K. The column with the largest magnitude corresponds to the next estimable parameter because the parameter associated with this column has the largest effect (of all of the remaining parameters) on the response variables, which is not correlated with the effects of the parameters that have already been selected.
7. Select the corresponding column in Z and augment the matrix X_K by including the new column. Denote the augmented matrix as X_{K+1}.
8. Advance the iteration counter by 1 and repeat steps 4−7 until the column of largest magnitude in the residual matrix is smaller than a prescribed cutoff value.

In step 4, the selected columns are used to construct a linear least-squares approximation to Z. Step 5 calculates the residual matrix, which excludes all of the information contained in the selected columns and the portion of the information contained in the remaining columns that is linearly correlated with the selected columns. By selecting the next most estimable parameter using the residual matrix, the effects of correlations among parameters belonging to the subset to be estimated are reduced. This parameter estimability ranking scheme is superior to that developed by Li et al.,[13] because it can accommodate dynamic models wherein some responses are available at irregular sampling times throughout each experimental run, and some responses (product properties) are available only at the end of the run.

Nomenclature

A = Cocatalyst, MAO
Ea_{kA} = Activation energy of active site reinitiation by ethylene after chain transfer to cocatalyst
Ea_{kds} = Activation energy of spontaneous deactivation
Ea_{kfdc} = Activation energy of active site formation
Ea_{kH} = Activation energy of active site reinitiation by ethylene after chain transfer to hydrogen
Ea_{ki} = Activation energy of active site initiation by ethylene
Ea_{kp} = Activation energy of propagation to ethylene
Ea_{kp1} = Activation energy of propagation to ethylene of active site type 1
Ea_{kp2} = Activation energy of propagation to ethylene of active site type 2
Ea_{ks} = Activation energy of active site reinitiation by ethylene after chain transfer to scavenger

Ea_{ktA} = Activation energy of chain transfer to cocatalyst of active sites with ethylene as terminal unit
Ea_{ktH} = Activation energy of chain transfer to hydrogen of active sites with ethylene as terminal unit
Ea_{ktM} = Activation energy of chain transfer to ethylene of active sites with ethylene as terminal unit
Ea_{ktS} = Activation energy of chain transfer to scavenger of active sites with ethylene as terminal unit
f_{c1} = Mol fraction of active site type 1 at the beginning of polymerization
f_{H2} = Hydrogen mole fraction gas phase
f_{H2} = Hydrogen mole fraction gas phase
F_{in} = Total feed rate of ethylene and hydrogen
$f_{in.M}$ = Mole fraction of ethylene in feed steam
$f_{in.H2}$ = Mole fraction of hydrogen in feed steam
H_2 = (1) Hydrogen (in model mechanisms); (2) Total unreacted hydrogen in reactor, mol (in mass balance)
h_{C2} = Henry's constant for ethylene
h_{H2} = Henry's constant for hydrogen
$[H_2]_{amr}$ = Ethylene concentration in amorphous polymer phase
HPD = Highest posterior distribution
k_A = Rate constant of active site reinitiation by ethylene after chain transfer to cocatalyst
$k_{A.ref}$ = Reference rate constant of active site reinitiation by ethylene after chain transfer to cocatalyst
k_{ds} = Rate constant of spontaneous deactivation of active sites with ethylene as terminal unit
$k_{ds.ref}$ = Reference rate constant of spontaneous deactivation of active sites with ethylene as terminal unit
k_{fdc} = Rate constant of active site formation
$k_{fdc.ref}$ = Reference rate constant of active site formation
k_H = Rate constant of active site reinitiation by ethylene after chain transfer to hydrogen
$k_{H.ref}$ = Reference rate constant of active site reinitiation by ethylene after chain transfer to hydrogen
k_i = Rate constant of active site initiation by ethylene
$k_{i.ref}$ = Reference rate constant of active site initiation by ethylene
k_p = Rate constant of propagation
k_{p1} = Rate constant of propagation of active site type 1
k_{p2} = Rate constant of propagation of active site type 2
$k_{p.ref}$ = Reference rate constant of propagation
k_S = Rate constant of active site reinitiation by ethylene after chain transfer to scavenger
$k_{S.ref}$ = Reference rate constant of active site reinitiation by ethylene after chain transfer to scavenger
k_{tA} = Rate constant of chain transfer to cocatalyst of active sites with ethylene as terminal unit
$k_{tA.ref}$ = Reference rate constant of chain transfer to cocatalyst of active sites with ethylene as terminal unit
k_{tH} = Rate constant of chain transfer to hydrogen of active sites with ethylene as terminal unit
$k_{tH.ref}$ = Reference rate constant of chain transfer to hydrogen of active sites with ethylene as terminal unit
k_{tM} = Rate constant of chain transfer to ethylene of active sites with ethylene as terminal unit
$k_{tM.ref}$ = Reference rate constant of chain transfer to ethylene of active sites with ethylene as terminal unit
k_{tS} = Rate constant of chain transfer to scavenger of active sites with ethylene as terminal unit
$k_{tS.ref}$ = Reference rate constant of chain transfer to scavenger of active sites with ethylene as terminal unit
M = (1) Ethylene (in model mechanisms); (2) Total unreacted ethylene inside reactor, mol (in mass balance)
$[M]_{amr}$ = Ethylene concentration in amorphous polymer phase
Mn = Number-average molecular weight
Mw = Weight-average molecular weight
$N(0)$ = Initial active site
$N(r)$ = Living polymer of chain length r
N^* = Potential active sites
$N_A(0)$ = Uninitiated active sites with cocatalyst attached
$N_H(0)$ = Uninitiated active sites with hydrogen attached
$N_S(0)$ = Uninitiated active sites with scavenger attached
PDI = Polydispersity
$Q(r)$ = Dead polymer of length r
R = Ideal gas constant
r_{HM} = Feed rate ratio of hydrogen to ethylene
S = Scavenger, Ti−BuAl
T = Reaction temperature
T_c = Critical temperature
Xi = ith moment of product
Yi = ith moment of active site

Literature Cited

(1) Soares, J. B. P.; Hamielec, A. E. General Dynamic Mathematical Modelling of Heterogeneous Ziegler−Natta and Metallocene Catalyzed Copolymerization with Multiple Site Types and Mass and Heat Transfer Resistances. *Polym. React. Eng*. **1995**, *3*, 261.

(2) Soares, J. B. P.; Hamielec, A. E. Effect of Reactor Residence Time Distribution on the Size Distribution of Polymer Particles Made with Heterogeneous Ziegler−Natta and Supported Metallocene Catalysts. A Generic Mathematical Model. *Macromol. Theory Simul.* **1995***, 4*, 1085.

(3) Xie, T.; McAuley, K. B.; Hsu, J. C. C.; Bacon, D. W. Modeling Molecular Weight Development of Gas-Phase Alpha-Olefin Copolymerization *AIChE J.* **1995**, *41*, 1251.

(4) Soares, J. B. P.; Hamielec, A. E. Bivariate Chain Length and Long Chain Branching Distribution for Copolymerization of Olefins and Polyolefin Chains Containing Terminal Double-Bonds. *Macromol. Theory Simul.* **1996**, *53*, 547.

(5) Soares, J. B. P.; Hamielec, A. E. Copolymerization of Olefins in A Series of Continuous Stirred-Tank Slurry-Reactors Using Heterogeneous Ziegler−Natta and Metallocene Catalysts. I. General Dynamic Mathematical Model. *Polym. React. Eng*. **1996**, *4*, 153.

(6) Shaw, B. M. Statistical Issues in Kinetic Modelling of Gas-Phase Ethylene Copolymerization. Ph.D. Thesis, Queen's University, Kingston, Ontario, Canada, 1999.

(7) Shaw, B. M.; McAuley, K. B.; Bacon, D. W. Simulation Joint Chain Length and Composition Fractions From Semi-Batch Ethylene Copolymerization. *Polym. React. Eng.* **1998**, *62*, 13.

(8) Khare, N. P.; Seavey, K. C.; Liu, Y. A.; Ramanathan, S.; Lingard, S.; Chen, C.-C. Steady-State and Dynamic Modeling of Commercial Slurry High-Density Polyethylene (HDPE) Processes. *Ind. Eng. Chem. Res.* **2002**, *41*, 5601.

(9) Khare, N. P.; Lucas, B.; Seavey, K. C.; Liu, Y. A.; Sirohi, A.; Ramanathan, S.; Lingard, S.; Song, Y.; Chen, C.-C. Steady-State and Dynamic Modeling of Gas-Phase Polypropylene Processes Using Stirred-Bed Reactors. *Ind. Eng. Chem. Res.* **2004**, *43*, 884.

(10) Matos, V.; Mattos Neto, A. G.; Pinto, J. C. Method for Quantitative Evaluation of Kinetic Constants in Olefin Polymerizations. I. Kinetic Study of a Conventional Ziegler−Natta Catalyst Used for Propylene Polymerizations. *J. Appl. Polym. Sci.* **2001**, *79*, 2076.

(11) Matos, V.; Mattos Neto, A. G.; Nele, M.; Pinto, J. C. Method for Quantitative Evaluation of Kinetic Constants in Olefin Polymerizations. II. Kinetic Study of a High-Activity Ziegler−Natta Catalyst Used for Bulk Propylene Polymerizations. *J. Appl. Polym. Sci.* **2002**, 86.

(12) Yao, K. Z.; Shaw, B. M.; Kou, B.; McAuley, K. B.; Bacon, D. W. Modeling Ethylene/Butene Copolymerization with Multi-Site Catalysts: Parameter Estimability and Experimental Design. *Polym. React. Eng.* **2003**, *11*, 563.

(13) Li, R.; Henson, M. A.; Kurtz, M. Selection of Model Parameters for Off-line Parameter Estimation. *IEEE Trans. Control Syst. Technol.* **2004**, *12*, 402.

(14) Kou, B.; McAuley, K. B.; Hsu, C. C. J.; Bacon, D. W.; Yao, K. Z. Gas-Phase Ethylene/Hexene Copolymerization with Metallocene Catalyst in a Laboratory-Scale Reactor. *Ind. Eng. Chem. Res*., in press.

(15) Kou, B. Mathematical Modelling of Gas-Phase Ethylene/Hexene Copolymerization with Metallocene Catalysts. Ph.D. Thesis, Queen's University, Kingston Ontario, Canada, 2004.

(16) Floyd, S.; Choi, K. Y.; Taylor, T. W.; Ray, W. H. Polymerization of Olefins through Heterogeneous Catalysis. III. Polymer Particle Modeling with an Analysis of Intraparticle Heat and Mass Transfer Effects. *J. Appl. Polym. Sci.* **1986**, *32*, 2935.

(17) Floyd, S.; Choi, K. Y.; Taylor, T. W.; Ray, W. H. Polymerization of Olefins through Heterogeneous Catalysis. IV. Modeling of Heat and Mass Transfer Resistance in the Polymer Particle Boundary Layer. *J. Appl. Polym. Sci.* **1986**, *31*, 2231.

(18) Floyd, S.; Hutchinson, R. A.; Ray, W. H. Polymerization of Olefins through Heterogeneous Catalysis. V: Gas−Liquid Mass Transfer Limitations in Liquid Slurry Reactors. *J. Appl. Polym. Sci.* **1986**, *32*, 5451.

(19) Floyd, S.; Heiskanen, T.; Taylor, T. W.; Mann, G. E.; Ray, W. H. Polymerization of Olefins through Heterogeneous Catalysis. VI. Effect of Particle Heat and Mass Transfer on Polymerization Behavior and Polymer Properties. *J. Appl. Polym. Sci.* **1987**, *334*, 1021.

(20) Floyd, S.; Heiskanen, T.; Ray, W. H. Solid Catalyzed Olefin Polymerization *Chem. Eng. Prog.* **1988**, *84*, 56.

(21) Hutchinson, R. A.; Ray, W. H. Polymerization of Olefins through Heterogeneous Catalysis. VIII. Monomer Sorption Effects. *J. Appl. Polym. Sci.* **1990**, *41*, 51.

(22) Moore, S. J.; Wanke, S. E. Solubility of Ethylene, 1-Butene and 1-Hexene in Polyethylenes. *Chem. Eng. Sci.* **2001**, *56*, 4121.

(23) Böhm, L. L. Reaction Model for Ziegler-Natta Polymerization Processes. *Polymer* **1978**, *19*, 545.

(24) Böhm, L. L. Ethylene Polymerization Process with a Highly Active Ziegler−Natta Catalyst: 1. Kinetics. *Polymer* **1978**, *19*, 553.

(25) Böhm, L. L. Ethylene Polymerization Process with a Highly Active Ziegler−Natta Catalyst: 2. Molecular Weight Regulation. *Polymer* **1978**, *19*, 562.

(26) McAuley, K. B.; MacGregor, J. F.; Hamielec, A. E. A Kinetic Model for Industrial Gas-Phase Ethylene Copolymerization. *AIChE J.* **1990**, *36*, 837.

(27) Stewart, W. E. *GREG*: *A FORTRAN Subroutine for Nonlinear Regression and Experimental Design, User's Manual*; University of Wisconsin, 1995.

(28) Tremblay, A. Parameter Estimation for Polymerization Reactor and Product Property Data: Missing Data Approach. Master Thesis, Queen's University, Kingston, ON, Canada, 1999.

(29) Bates, D. M.; Watts, D. G. *Nonlinear Regression Analysis and Its Applications*; John Wiley & Sons: New York, 1988.

(30) Chakravarti, S.; Ray, W. H. Kinetic Study of Olefin Polymerization with a Supported Metallocene Catalyst. II. Ethylene/1-Hexene Copolymerization in Gas Phase. *J. Appl. Polym. Sci.* **2001**, *80*, 1096.

(31) Chakravarti, S.; Ray, W. H.; Zhang, S. X. Kinetic Study of Olefin Polymerization with a Supported Metallocene Catalyst. IV. Comparison of Bridged and Unbridged Catalyst in Gas Phase. *J. Appl. Polym. Sci*. **2001**, *81*, 1451.

(32) Galvan, R.; Tirrell, M. Molecular Weight Distribution Predictions for Heterogeneous Ziegler−Natta Polymerization Using a Two-Site Model. *Chem. Eng. Sci.* **1986**, *41*, 2385.

(33) Wang, Q.; Weng, J. H.; Xu, L.; Fan, Z. Q.; Feng, L. X. Multiple Active Sites Model of Ethylene Polymerization with the Cp_2ZrCl_2−Aluminoxanes Catalytic System. *Polymer* **1999**, *40*, 1863.

(34) Kaminsky, W.; Renner, F. High Melting Polypropenes by Silica-Supported Zirconocene Catalysts. *Macromol. Rapid Commun.* **1993**, *14*, 239.

(35) Sacchi, M. A.; Zucchi, D.; Tritto, I.; Locatelli, P.; Dall'Occo, T. Silica-supported Metallocenes: Stereochemical Comparison between Homogeneous and Heterogeneous Catalysts. *Macromol. Rapid Commun.* **1995**, *16*, 581.

(36) Chu, K. J.; Shan, C. L. P.; Soares, J. B. P.; Penlidis, A. Copolymerization of Ethylene and 1-Hexene with In Situ Supported $Et[Ind]_2ZrCl_2$. *Macromol. Chem. Phys*. **1999**, *200*, 2372.

(37) Marques, M. D. V.; Conte, A.; Resende, F. C.; Chaves, E. G. Copolymerization of Ethylene and 1-Octene By Homogeneous and Different Supported Metallocenic Catalysts. *J. Appl. Polym. Sci.* **2001**, *82*, 724.

(38) Soga, K.; Kaminaka, M. Copolymerization of Olefins with SiO_2-, Al_2O_3- and $MgCl_2$-Supported Metallocene Catalysts Activated by Trialkylaluminiums. *Macromol. Chem. Phys.* **1994**, *195*, 1369.

(39) Soga, K.; Kaminaka, M. Polymerization of Propene with a *rac*-$(CH_3)_2Si(2,4\text{-}(CH_3)_2C_5H_3)(3',5'\text{-}(CH_3)_2C_5H_3)ZrCl_2$/MAO/$SIO_2$−$Al(iC_4H_9)_3$ Catalyst System. *Macromol. Rapid Commun*. **1994**, *15*, 593.

(40) Chu, K. J.; Soares, J. B. P.; Penlidis, A. Effect of Experimental Conditions on Ethylene Polymerization with In Situ-Supported Metallocene Catalyst. *J. Polym. Sci, Part A*: *Polym. Chem.* **2000**, *38*, 1803.

(41) Kumkaew, P.; Wu, L.; Praserthdam, P.; Wanke, S. E. Rates and Product Properties of Polyethylene Produced By Copolymerization of 1-Hexene and Ethylene In the Gas Phase with $(n\text{-}BuCp)_2ZrCl_2$ on Supports with Different Pore Sizes. *Polymer* **2003**, *44*, 4791.

(42) Yermakov; Yu, I.; Kuznetsov, B. N.; Zakharov, V. A. *Catalysis by Supported Complexes*; Elsevier: Amsterdam, 1981; p 59.

(43) Nowlin, T. E.; Mink, R. L.; Lo, F. Y.; Kumar, T. Ziegler−Natta Catalysts on Silica for Ethylene Polymerization. *J. Polym. Sci. Part A*: *Polym. Chem.* **1991**, *29*, 1167.

Received for review October 27, 2004
Revised manuscript received January 11, 2005
Accepted January 14, 2005

IE048957O